27. Recent experimental results confirm that ridges in the floor of a channel do generate transverse components in electroosmotic flows (*28*).
28. T. J. Johnson, D. Ross, L. E. Locascio, *Anal. Chem.* 10.1021/ac010895d.
29. We drove flow in the channels by applying a constant pressure at the inlet reservoir with compressed air. We imaged the evolution of fluorescent streams in the channels using a Leica TCS confocal microscope with a 40×/1.0 numerical aperture objective.
30. Labeled polymers were prepared by allowing poly(ethylenimine) (molecular weight ~500,000) to react with fluorocein isothiocyanate. The product was dialyzed for several days. Diffusivities were calculated based on the broadening of fluorescent streams of the dye in confocal images flows of known speed: $D = 4 \times 10^{-6}$ cm²/s in water and $D = 2 \times 10^{-8}$ cm²/s in 80% glycerol/20% water. Flow speeds were measured by weighing the fluid collected at the outlet of the channel. Viscosity of the glycerol/water solution was estimated to be 0.67 g/cm·s by comparing the flow rate to that of water through the same channel with the same applied pressure.

31. Supported by Defense Advanced Research Projects Agency grants NSF ECS-9729405 and NSF DMR-9809363 Materials Research Science and Engineering Center (A.D.S., S.K.W.D., H.A.S., and G.M.W.); NIH grant GM51559 (A.D.S., S.K.W.D, and G.M.W.); Army Research Office grant DAAG55-97-1-0114 (H.A.S.); and NSF-9875933, NSF DMS-9803555, and a Sloan Foundation Fellowship (I.M.). S.K.W.D. thanks the Deutsche Forschungsgemeinschaft for a research fellowship.

13 September 2001; accepted 14 December 2001

A Group-IV Ferromagnetic Semiconductor: Mn_xGe_{1-x}

Y. D. Park,* A. T. Hanbicki, S. C. Erwin, C. S. Hellberg, J. M. Sullivan, J. E. Mattson,† T. F. Ambrose,‡ A. Wilson,§ G. Spanos, B. T. Jonker‖

We report on the epitaxial growth of a group-IV ferromagnetic semiconductor, Mn_xGe_{1-x}, in which the Curie temperature is found to increase linearly with manganese (Mn) concentration from 25 to 116 kelvin. The *p*-type semiconducting character and hole-mediated exchange permit control of ferromagnetic order through application of a ±0.5-volt gate voltage, a value compatible with present microelectronic technology. Total-energy calculations within density-functional theory show that the magnetically ordered phase arises from a long-range ferromagnetic interaction that dominates a short-range antiferromagnetic interaction. Calculated spin interactions and percolation theory predict transition temperatures larger than measured, consistent with the observed suppression of magnetically active Mn atoms and hole concentration.

Ferromagnetic (FM) semiconductors are materials that simultaneously exhibit semiconducting properties and spontaneous long-range FM order. Classic examples include the europium chalcogenides and the chalcogenide spinels, both extensively studied several decades ago (*1*). The coexistence of these properties in a single material provides fertile ground for fundamental studies (*2*). However, device applications have languished because of low magnetic ordering (Curie) temperatures and the inability to incorporate these materials in thin film form with mainstream semiconductor device materials.

Interest in ferromagnetic semiconductors (FMSs) was rekindled with the discovery of spontaneous FM order in $In_{1-x}Mn_xAs$ in 1989 (*3*) and in $Ga_{1-x}Mn_xAs$ in 1996 (*4*–*6*), when FM properties were realized in semiconductor hosts already widely recognized for semiconductor device applications. These new FMS materials exhibit Curie temperatures up to 35 K and 110 K, respectively, for Mn concentrations of order 5% and sufficiently high hole densities and have been closely studied for their potential in future spin-dependent semiconductor device technologies. For example, $Ga_{1-x}Mn_xAs$ has been used as a source of spin-polarized carriers in both light-emitting diodes (*7*) and resonant tunneling diode heterostructures (*6*, *8*). Electric field control of FM order has recently been reported in $In_{1-x}Mn_xAs$ heterostructures (*9*), demonstrating one of the unique properties of these materials and portending a host of new applications. Experimental evidence for Curie temperatures above 300 K has been reported in other materials, such as $CdMnGeP_2$ (*10*).

We report on the preparation of a group-IV FM semiconductor, Mn_xGe_{1-x}. Although most experimental work on FMS has focused on III-V and II-VI compounds, there is broad interest in the group-IV semiconductors, C, Si, Ge, and $Si_{1-x}Ge_x$. A mean-field solution of a Zener model has recently predicted that FM order can be stabilized in these and other diluted magnetic semiconductor families as well (*11*–*13*). We grew single-crystal Mn_xGe_{1-x}(001) films on both Ge and GaAs(001) substrates. These films have Curie temperatures in the range 25 to 116 K for $0.006 \leq x \leq 0.035$, are *p*-type with carrier densities of $\sim 10^{19}$ to 10^{20} cm^{-3}, and exhibit a pronounced extraordinary Hall effect. Mn_xGe_{1-x} has electronic and magnetic properties that are very promising for FMS device applications. The temperature dependence of the resistivity is semiconducting in character rather than metallic, and the holes mediate the FM exchange, as demonstrated in gated structures where control of the hole density results in corresponding control of FM order at gate voltages compatible with present complementary metal-oxide-semiconductor (CMOS) technology (±0.5 V). In addition, Ge is closely lattice matched to the $Al_yGa_{1-y}As$ family and has higher intrinsic hole mobilities than either GaAs or Si.

A group-IV host may also provide the simplest system for studying the fundamental origins of FM order. To this end, we used density-functional theory to study the electronic structure and magnetic interactions in Mn_xGe_{1-x}, with the aim of providing a first-principles foundation for future model descriptions. We find a strong short-range antiferromagnetic interaction between Mn spins competing with a long-range FM interaction that dominates at all Mn-Mn distances beyond nearest neighbor. From our calculated spin coupling constants and interaction range, we use percolation theory to predict the dependence of the Curie temperature on Mn concentration; the results suggest that a substantial fraction of the Mn does not participate in the FM ordering, consistent with our experimental data.

As with the III-Mn-V FMS compounds, the low solubility of Mn in Ge requires nonequilibrium growth techniques at reduced substrate temperatures to minimize phase separation or the formation of unwanted compounds (*3*–*6*, *14*). The samples were grown by molecular beam epitaxy from elemental Knudsen cell sources at a growth rate of ~5 Å/min. After thermal desorption of the GaAs or Ge(001) substrate surface oxide at ~590°C, a thin buffer layer of Ge was grown at a substrate temperature of 250°C. The substrate temperature was reduced further to 70°C for the growth of Mn_xGe_{1-x} to a typical thickness of 1000 Å to avoid formation of bulk phase precipitates (which plague the III-Mn-V compounds) (*4*, *15*). Reflection high-energy electron diffraction

Naval Research Laboratory, Washington, DC 20375, USA.

*Present address: School of Physics and CSCMR, Seoul National University, Seoul 151-747, Korea.
†Present address: Micron Technology, Boise, ID 33707, USA.
‡Present address: Seagate Technology, Pittsburgh, PA 15203, USA.
§Present address: Boeing Satellite Systems, El Segundo, CA 90009, USA.
‖To whom correspondence should be addressed. E-mail: jonker@nrl.navy.mil

patterns exhibited a streaky 2×1 reconstruction throughout the growth of both the buffer layer and Mn_xGe_{1-x} film, indicating predominantly two-dimensional growth. X-ray diffraction data revealed no phases other than that of the host Ge lattice and confirmed that the crystallographic axes of the films were commensurate with those of the substrate. The Mn concentration was determined from x-ray fluorescence together with microprobe analysis with energy-dispersive x-ray spectroscopy measurements on a transmission electron microscope. Despite the low growth temperature, Mn diffusion/phase separation resulted in small precipitates of 2 to 6 nm in diameter with a Mn concentration higher than that of the surrounding matrix. However, the Mn concentration of these precipitates was measured to be ~10 to 15%, which does not correspond to any known magnetic phase. In contrast, phase separation in GaMnAs and GaMnSb leads to the formation of bulk phase precipitates (MnAs and MnSb), with Curie temperatures (T_c) of 40° and 312°C, respectively. Growth of Mn_xGe_{1-x} at higher substrate temperatures (300° to 350°C) indeed results in the formation of FM $Mn_{11}Ge_8$ nanoclusters with a T_c near room temperature, as described elsewhere (*16*). The Mn concentrations quoted below are those of the homogeneous matrix. Moderate annealing of the samples at temperatures up to 200°C has no effect on the structural, magnetic, and transport properties.

The magnetic properties of the samples were determined from superconducting quantum interference device magnetometry and magnetotransport measurements. Magnetization loops show hysteretic behavior and substantial remanence (Fig. 1, inset), with saturation magnetizations up to 30 emu/cm^3. These values correspond to ~1.4 to 1.9 Bohr magnetons (μ_B) per Mn atom if all contribute equally or to a magnetically active fraction 45 to 60% if each Mn atom has the full theoretical moment of 3 μ_B (as discussed below). For comparison, the magnetically active fraction of Mn atoms in $Ga_{1-x}Mn_xAs$ is about 13% (*17*). The remanence exhibits no temporal dependence, as expected for an FM alloy rather than a spin-glass phase. The temperature dependence of the magnetization for a sample with $x = 0.02$ shows that no signal is detected near room temperature for any of the samples, confirming the absence of any known FM phases of Mn_yGe_{1-y}, all of which are Mn-rich with Curie temperatures near or above room temperature (*14*, *16*). The shape of the curve differs from the Brillouin behavior expected for a classic ferromagnet. This deviation has also been observed in $Ga_{1-x}Mn_xAs$ films and attributed to the presence of multiple exchange interactions (*18*). The Curie temperature is therefore estimated from a Curie-Weiss fit to the data as the magnetization approaches zero and shows a linear dependence on Mn concentration (Fig. 2A). The value of T_c for a given Mn concentration is higher than that predicted by a mean-field Zener model (*11*, *12*) but lower than that obtained from our percolation calculation based on first-principles spin interactions.

The resistivity (r) of the Mn_xGe_{1-x} films decreases with temperature for all Mn concentrations studied (Fig. 2B). At very dilute Mn concentrations below that required to stabilize FM order, the dominant conductivity mechanism is hopping (*16*). This persists for the higher concentrations studied here for a broad range of temperatures below T_c, as indicated by a linear dependence of log r on $T^{-1/4}$. Hole densities obtained from room temperature Hall measurements increase with Mn concentration and range from 10^{19} to 10^{20} cm^{-3}. However, these values underestimate the true hole density due to the presence of the extraordinary Hall effect (EHE) (*19*), which produces an additional contribution to the Hall voltage proportional to the sample's magnetization. Data from films on Ge substrates are complicated by contributions from the substrate, which become substantial above 150 K (*16*). The effect of critical scattering, which is typically manifested as a local maximum near T_c, is probably suppressed by increased impurity scattering due to outdiffused Ga (*20*).

All of the samples exhibit a substantial EHE that dominates at low to moderate magnetic fields, characteristic of a FMS matrix (*15*). Figure 3A shows a plot of the Hall voltage as a function of applied field at various temperatures for a $Mn_{0.023}Ge_{0.977}$ film on Ge(001). The EHE signal is smaller at 10 K, which we attribute to the nonmetallic character of the sample—the hole density is lower at lower temperature, as is evident from the smaller slope at higher fields, where the Hall voltage is proportional to carrier density. This behavior is different from data published for GaMnAs samples that were metallic in character (*6*), in which the hole density showed little temperature dependence. Similar data are obtained for films grown on GaAs(001) substrates, although the EHE is not as pronounced. This difference is attributed to outdiffusion of Ga atoms from the substrate and into the film where they act as acceptors (*20*), which results in increased impurity scattering, suppressing the effect of skew scattering and the consequent EHE. The Mn_xGe_{1-x}/GaAs samples exhibit slightly higher hole densities (<10%) for a given Mn concentration but exhibit no measurable difference in Curie temperatures, which again can be at-

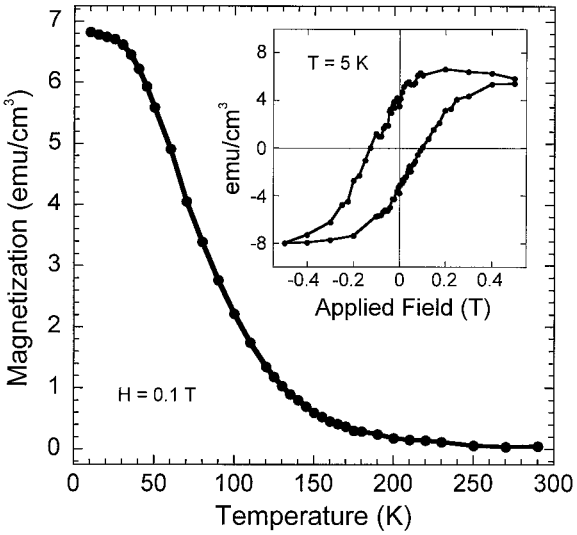

Fig. 1. Temperature dependence of the magnetization for a 615 Å thick $Mn_{0.02}Ge_{0.98}$ film (applied field = 0.1 T). The inset shows the B-H loop at 5 K for the same sample.

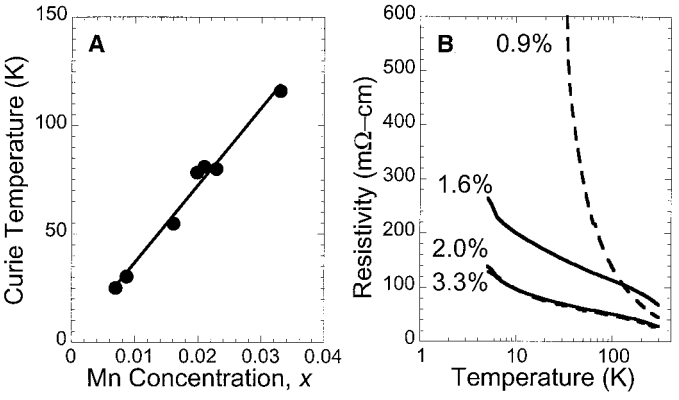

Fig. 2. (**A**) Dependence of T_c on the Mn concentration of the FM Mn_xGe_{1-x} matrix. (**B**) Temperature dependence of the resistivity for several Mn_xGe_{1-x} films on GaAs(001) for the Mn concentrations noted.

tributed to increased impurity scattering. The Hall voltage does not saturate for applied fields up to 9 T, making an accurate determination of hole densities difficult. Although EHE data and a corresponding Arrott plot analysis can be used to determine the true Curie temperature of magnetic semiconductor films if the resistivity of the sample is metallic in character (as is typically the case for $Ga_{1-x}Mn_xAs$), the localization effects that accompany the semiconducting character of the Mn_xGe_{1-x} films make such an analysis unreliable (*6*, *21*, *22*).

The nonmetallic character permits control of carrier density in simple gated structures through application of a small gate voltage. If the FM exchange is mediated by the holes as in the III-Mn-V compounds (*11*, *12*), this should result in control of the FM order, as has been demonstrated for $In_{1-x}Mn_xAs$ (*9*). Gated Hall bars were fabricated with a multilayer structure consisting of a Ge buffer layer, a 600 Å $Mn_{0.015}Ge_{0.985}$ active layer ($T_c \sim 50$ K), and a sputter deposited, 1200 Å thick SiN_x film as the gate insulator. Room temperature measurements confirmed that the channel current could be varied by over 30% for gate voltages of ±10 V. The EHE was used to monitor the effect of gate voltage on FM order and is enhanced (suppressed) as the hole density is enhanced (suppressed) by the ±0.5-V gate voltage (Fig. 3B), confirming that FM exchange is hole-mediated in Mn_xGe_{1-x}. The field dependence of the EHE signal is different than that observed for $Mn_{0.023}Ge_{0.977}$ in Fig. 3A because of the more insulating character of the $Mn_{0.015}Ge_{0.985}$ sample. Similar behavior has been observed for GaMnAs (*22*). The FM order is modulated at higher temperatures (50 K compared with 22 K) and substantially smaller gate voltages (0.5 V compared with 125 V) than required for $In_{1-x}Mn_xAs$ (*9*). These low gate voltages demonstrate that electric field controlled FM order, a unique property of FMS compounds, can be incorporated with conventional low voltage circuitry.

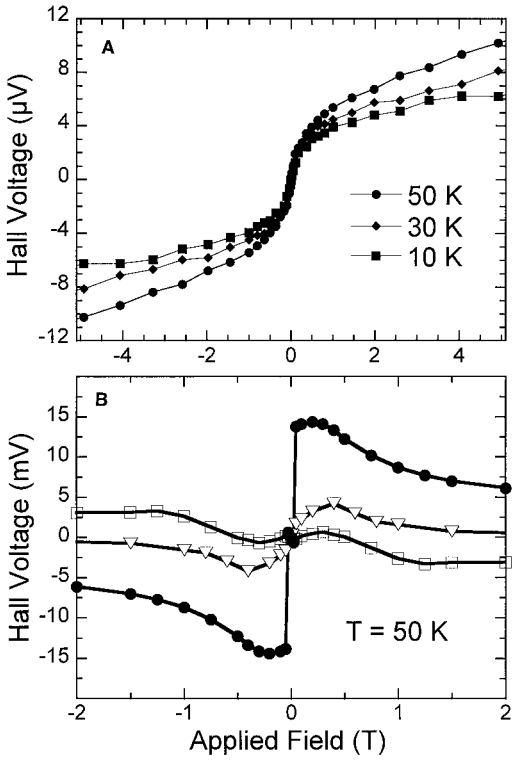

Fig. 3. (**A**) Hall voltage versus applied magnetic field at various temperatures for a $Mn_{0.023}Ge_{0.977}$ film on Ge(001). The extraordinary Hall effect dominates at low fields and prevents an accurate determination of hole density. (**B**) Hall voltage versus applied magnetic field at 50 K in a gated Hall bar, where a ±0.5-V gate voltage is used to vary the hole density in the $Mn_{0.015}Ge_{0.985}$ active layer. At zero gate voltage (triangles), a small EHE signal is observed. As the hole density in the MnGe layer is enhanced (solid circles) or suppressed (squares) by the gate voltage, the EHE signal and corresponding FM order are enhanced or suppressed. Different Hall bar dimensions and film thicknesses were used in (A) and (B).

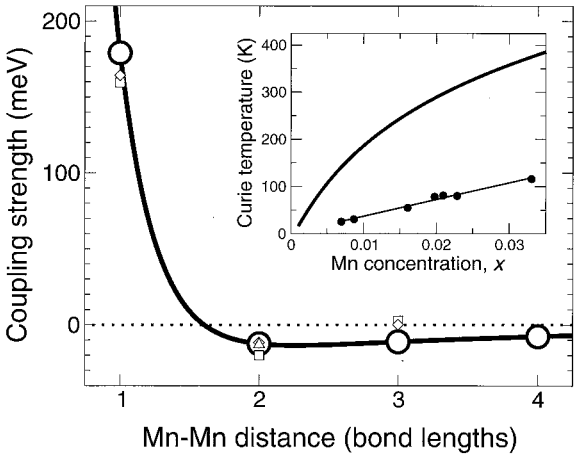

Fig. 4. Theoretical spin-spin coupling strength in Mn_xGe_{1-x} as a function of Mn-Mn distance. Large circles: coupling strength for two Mn per 32-atom cell; solid curve: analytic fit of Eq. 1. Other symbols: coupling strengths from two, three, and four Mn per cell at concentrations between 3.7 and 7.4%. (**Inset**) Theoretical Curie temperature as a function of Mn concentration, obtained from DFT spin coupling strengths (Eq. 1) and the percolation expression for T_c (Eq. 2). Also shown are the experimental Curie temperatures from Fig. 1 (solid circles).

To investigate the microscopic origins of ferromagnetism in Mn_xGe_{1-x}, we turned to electronic-structure calculations based on density-functional theory (DFT). We modeled Mn_xGe_{1-x} using periodic supercells—total energies and forces were calculated within the local-spin-density approximation (LSDA) with norm-conserving pseudopotentials (*23*) and a plane-wave basis with a kinetic-energy cutoff of 50 Ry (*24*). Mn impurities preferentially occupy the substitutional site, where the defect formation energy is 0.7 eV less than for the interstitial site. An isolated substitutional Mn creates only negligible distortion of the host lattice, with neighboring Ge atoms perturbed by less than 0.05 Å. The electronic configuration of atomic Mn is $3d^54s^2$; thus, for a Mn^{2+} impurity in Ge, one might expect a magnetic moment of $5\mu_B$ due to strong Hund coupling. However, we find that strong hybridization between Mn *d* states of T_2 symmetry with Ge *p* states leads to the configuration $e(\uparrow)^2\ T_2(\uparrow)^2\ T_2(\downarrow)^1$, with a magnetic moment of $3\mu_B$, in agreement with other DFT studies (*25*, *26*).

To understand the origin of FM order in the Mn_xGe_{1-x} system, we analyzed the interactions between Mn spins using the spin Hamiltonian $H = \Sigma J_{ij}\mathbf{S}_i\cdot\mathbf{S}_j$. The spin coupling constants, J_n, were determined from DFT calculations with two Mn atoms in a 32-atom supercell, equivalent to a Mn concentration $x = 0.063$. The two Mn atoms, located at various separations within the unit cell, were initialized with parallel or antiparallel spin polarization. At self-consistency, both spin configurations remained stable for all Mn-Mn separations, with the moment per Mn again very close to $3\mu_B$, regardless of the Mn relative positions or concentration. From the difference in LSDA total energies, we obtain J_n for two Mn atoms separated by *n* bonds along a bonding chain, plotted in Fig. 4 for $n =$ 1 through 4. The interactions are strongly antiferromagnetic ($J_n > 0$) for nearest-neighbor Mn and weakly FM ($J_n < 0$) for all separations beyond nearest neighbor. These values show little dependence on Mn concentration or clustering. We fit these numerical results to the analytic expression

$$J(r) = J_{AF}\exp(-r/r_{AF}) + J_{FM}\exp(-r/r_{FM}) \quad (1)$$

shown as a solid curve. The FM interaction range, $r_{FM} = 5.0$ Å, is much larger (by a factor of ~10) than the antiferromagnetic

interaction range, r_{AF}, as expected. These results are consistent with a short-range superexchange mechanism competing with a long-range kinetic-exchange mechanism.

Uniformly distributed ferromagnetically aligned Mn is thermodynamically more stable than all other configurations we have considered, with one exception: antiferromagnetic nearest-neighbor Mn dimers, for which the relative formation energy is −83 meV. This energy gain represents a driving force for reducing the amount of Mn available for ordering ferromagnetically. Thus, for a given total Mn concentration, the formation of AF Mn dimers will reduce the effective Mn concentration and T_c.

Finally, we address the predicted dependence of the Curie temperature on Mn concentration. At experimentally accessible concentrations, the average Mn-Mn separation is much larger than the FM interaction range, r_{FM}. This limits the applicability of mean-field theory for calculating the transition temperature, so we use a percolation approach (*27*), in which T_c is given by

$$k_B T_c = S(S + 1)J(R_{perc}), \qquad (2)$$

where k_B is the Boltzmann constant, S is the Mn spin (3/2), and R_{perc}, the radius of a ferromagnetically ordered Mn cluster at the percolation threshold, is proportional to the average Mn-Mn separation. Using the functional form in Eq. 1 for $J(r)$, we show in Fig. 4 (inset) the predicted dependence of the Curie temperature on Mn concentration for low concentrations (at higher concentrations, the short-range AF interactions become important, so that at its maximum near $x = 0.14$, the predicted T_c is only 50% higher than at $x = 0.035$). Although the behavior is qualitatively similar to that measured for the range of experimental compositions covered, the predicted temperatures are larger by roughly a factor of 4. This difference is due to three effects. First, the magnetization data indicate a magnetically active fraction of only 45 to 60%, which we attribute in part to the predicted formation of AF nearest-neighbor Mn dimers, effectively suppressing the measured Curie temperatures for a given concentration. The second effect is the well-known tendency of the LSDA to overestimate spin coupling strengths in antiferromagnetic insulators by factors ranging between 3 (*28*) and 6 (*29*); for kinetic exchange in a FM metal, this effect may be smaller but should still be present. The third effect is the absence of any hole compensation in our theory, which leads to theoretical hole densities of order 10^{22} cm^{-3}. This is far larger than the measured carrier concentrations ($\sim 10^{19}$ to 10^{20} cm^{-3}) and likely results in a further overestimate of the FM interaction strength. These considerations reconcile the difference between the experimental and predicted values and suggest avenues to improve our predictive ability in these complex materials.

References and Notes

1. C. Haas, *CRC Crit. Rev. Solid State Sci.* **1**, 47 (1970).
2. E. L. Nagaev, *Phys. Stat. Solidi B* **145**, 11 (1988).
3. H. Munekata *et al.*, *Phys. Rev. Lett.* **63**, 1849 (1989).
4. J. De Boeck *et al.*, *Appl. Phys. Lett.* **68**, 2744 (1996).
5. H. Ohno *et al.*, *Appl. Phys. Lett.* **69**, 363 (1996).
6. H. Ohno *et al.*, *Science* **281**, 951 (1998).
7. Y. Ohno *et al.*, *Nature* **402**, 790 (1999).
8. T. Hayashi *et al.*, *J. Appl. Phys.* **87**, 4673 (2000).
9. H. Ohno *et al.*, *Nature* **408**, 944 (2000).
10. G. A. Medvedkin *et al.*, *Jpn. J. Appl. Phys.* **39**, L949 (2000).
11. T. Dietl, H. Ohno, F. Matsukura, J. Cibert, D. Ferrand, *Science* **287**, 1019 (2000).
12. T. Dietl, H. Ohno, F. Matsukura, *Phys. Rev. B* **63**, 195205 (2001).
13. A discussion of the terminology can be found on *Science* Online at www.sciencemag.org/cgi/content/full/295/5555/651/DC1.
14. T. B. Massalaski, Ed., *Binary Alloy Phase Diagrams* (American Society for Metals, Metals Park, OH, ed. 2, 1990), vol. 2, p. 1964.
15. E. Abe, F. Matsukura, H. Yasuda, Y. Ohno, H. Ohno, *Physica E* **7**, 981 (2000).
16. Y. D. Park *et al.*, *Appl. Phys. Lett.* **78**, 2739 (2001).
17. H. Ohldag *et al.*, *Appl. Phys. Lett.* **76**, 2928 (2000).
18. A. Van Esch *et al.*, *Phys. Rev. B* **56**, 13103 (1996).
19. T. Omiya *et al.*, *Physica E* **7**, 976 (2000).
20. T. Maeda, H. Tanaka, *J. Cryst. Growth* **201–202**, 194 (1999).
21. F. Matsukura, H. Ohno, A. Shen, Y. Sugawara, *Phys. Rev. B* **57**, R2037 (1998).
22. Y. Iye *et al.*, *Mat. Sci. Eng. B* **63**, 88 (1999).
23. M. Fuchs, M. Scheffler, *Comput. Phys. Commun.* **119**, 67 (1999).
24. The ABINIT code is a common project of the Université Catholique de Louvain, Corning Incorporated, and other contributors (www.pcpm.ucl.ac.be/ABINIT).
25. T. C. Schulthess, W. H. Butler, *J. Appl. Phys.* **89**, 7021 (2001).
26. M. van Schilfgaarde, O. N. Mryasov, *Phys. Rev. B* **63**, 233205 (2001).
27. V. I. Litvinov, V. K. Dugaev, *Phys. Rev. Lett.* **86**, 5593 (2001).
28. J. Kortus, C. S. Hellberg, M. R. Pederson, *Phys. Rev. Lett.* **86**, 3400 (2001).
29. R. L. Martin, F. Illas, *Phys. Rev. Lett.* **79**, 1539 (1991).

30. This work was supported by the Office of Naval Research and the Defense Advanced Research Projects Agency Spins in Semiconductors program. Y.D.P., A.T.H., J.M.S., and T.F.A. are National Research Council Postdoctoral Associates. A.W. is an American Society for Engineering Education Postdoctoral Associate.

18 September 2001; accepted 21 December 2001

Nanocrystallization During Nanoindentation of a Bulk Amorphous Metal Alloy at Room Temperature

J.-J. Kim,[1] Y. Choi,[1] S. Suresh,[1]* A. S. Argon[2]

It is known that nanocrystallites can form in shear bands produced during severe bending or high-energy ball milling of thin ribbons of a metallic glass. We present direct experimental evidence that highly confined and controlled local contact at the ultrafine scale in the form of quasi-static nanoindentation of a bulk glassy metal alloy at room temperature can also cause nanocrystallization. Atomic force microscopy and transmission electron microscopy show that nanocrystallites nucleate in and around shear bands produced near indents and that they are the same as crystallites formed during annealing without deformation at 783 kelvin. Analogous to results from recent experiments with glassy polymers, our results are reasoned to be a consequence of flow dilatation inside the bands and of the attendant, radically enhanced, atomic diffusional mobility inside actively deforming shear bands.

The structure, thermodynamic stability, and electrical and magnetic properties of thin ribbons of amorphous metal alloys have been the focus of many theoretical and experimental investigations (*1–6*). With the development of techniques to produce bulk metallic glasses, the mechanical properties of amorphous alloys have also become topics of scientific and technological interest (*7–13*) in terms of structural and functional applications. Bulk amorphous alloys exhibit unique properties: high strength, localized deformation by shear banding, paucity of strain hardening, and much higher hardness than crystalline alloys of comparable elastic modulus. Because glassy alloys do not exist in thermodynamic equilibrium, they undergo crystallization with the supply of thermal energy.

Experiments have also shown that severe bending of thin ribbons of amorphous glasses can lead to the formation of shear bands within which nanocrystallites could be nucleated (*6*). In addition, high-energy ball milling or mechanical alloying of thin ribbons of some Al-based amorphous metals has been found to induce

[1]Department of Materials Science and Engineering, [2]Department of Mechanical Engineering, Massachusetts Institute of Technology, Cambridge, MA 02139–4307, USA.

*To whom correspondence should be addressed. E-mail: ssuresh@mit.edu